Novel Nano-structured Metal–Semiconductor–Metal Photodetector with High Peak Voltage

Tomoko Borsa, Dylan F. Williams[1], Paul D. Hale[1], and Bart Van Zeghbroeck

Department of Electrical, Computer and Energy Engineering, University of Colorado at Boulder, 425 UCB, Boulder, CO 80309, U.S.A.
[1]*The National Institute of Standards and Technology, Boulder, CO 80305, U.S.A.*

Received December 1, 2008; accepted January 12, 2009; published online June 22, 2009

A novel nano-structured metal–semiconductor–metal photodetector consisting of interdigitated metal fingers and nanodots is successfully fabricated on a semi-insulating GaAs substrate by electron beam lithography, and integrated with an on-chip ground–signal–ground coplanar transmission line for pulse response measurements. The fabricated nano-structured metal–semiconductor–metal photodetector can be operated at 5 V, more than three times higher than the operating voltage of the regular metal–semiconductor–metal photodetector composed of narrowly spaced interdigitated electrodes only. Its dark current is lower than 0.5 nA until the bias voltage approaches the breakdown voltage. More importantly, it demonstrates a more than three times higher peak voltage output than that of the regular metal–semiconductor–metal photodetector while maintaining approximately a 10 ps pulse width that is limited by the bandwidth of the measurement setup, not by the speed of the photodetector. The transit model simulation indicates that the amplitude of the pulse response is strongly influenced by the voltage collapse across the photodetector.

DOI: 10.1143/JJAP.48.06FD03

1. Introduction

Photodetectors are commonly used to generate short electrical pulses by optoelectronic conversion of optical pulses. After all, ultrafast optical pulses are readily available with record pulse width less than 10 fs and peak power levels as large as 1.5 MW.[1)] Photodetectors fabricated on materials with short carrier recombination time such as low-temperature-grown GaAs are frequently used for this purpose, enabling the generation of electrical signals with THz bandwidth.[2)] Other types of photodetectors including p–i–n and metal–semiconductor–metal (MSM) photodetectors have been demonstrated with bandwidths well above 400 GHz[3)] without the need to reduce the carrier recombination time.

Since their first introduction around 1975,[4)] MSM photodetector devices have been used in high speed optoelectronic applications including fiber-optic links and wireless communication systems.[5)] A MSM photodetector is composed of interdigitated metal fingers on a semiconductor resulting in a large photosensitive area and a short transit time. The photodetector produces electrical signals by photogenerated carriers that drift towards the metal fingers. The MSM photodetector's low capacitance, high bandwidth and the compatibility with standard GaAs-based electronic circuits are the primary advantages over p–i–n photodiodes.[6)] More recently the MSM photodetector has been investigated as a potential device for microwave, millimeter-wave or even terahertz-wave applications as the response of MSM photodetector has steadily improved. With the latest advances in semiconductor processing technologies and proper design, it is possible to fabricate an MSM photodetector device that can be used as an ultrafast signal source.

The speed of MSM photodetectors is determined by two factors: the carrier recombination time and the intrinsic carrier transit time between the electrodes. Recombination-time-limited MSM photodetectors are made on a material with a very short recombination time such as low-temperature-grown GaAs. A high density of recombination centers is introduced during its low-temperature growth. Unfortunately this significantly reduces the sensitivity of the photodetector. When a MSM photodetector is made on a material with a long recombination time, the speed is controlled by the distance the carriers must traverse before arriving at an electrode. Therefore the speed of MSM photodetectors is improved by reducing the electrode spacing to nanometer scale, minimizing the intrinsic transit time. Interdigitated electrode structures, such as the one shown in Fig. 1 are often used to increase the optical absorption area of the detector while maintaining a short distance between the electrodes. However, the RC time constant of the device can also be the dominant factor because of the capacitance of the electrodes that are spaced on the nano-meter scale. For example,[3)] the measured bandwidth of an MSM photodetector with 100 nm finger spacing was shown to be less than the measured bandwidth with a 300 nm spacing for the detectors of the same size. In order to reduce *both* the intrinsic transit time and the RC time simultaneously, the overall area of a MSM photodetector must also to be small.

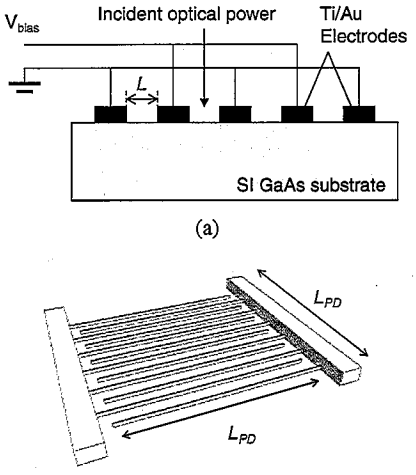

Fig. 1. (Color online) MSM photodetector with interdigitated electrodes constructed on a semi-insulating GaAs substrate: (a) cross sectional schematic view and (b) bird's eye view.

For many applications, MSM photodetectors need not only a fast temporal response, but also must generate a high peak output power. Common high speed measurement systems usually have a fixed impedance, typically 50 Ω. In these systems, the only possible way to obtain high power is by realization of a high output voltage. However, the conventional MSM photodetectors have a very small absorption volume, and it is thus not easy to obtain high output current. Additionally such photodetectors are generally forced to operate at a lower bias voltage due to the high field strength between the fingers, which causes dielectric breakdown at relatively low applied voltages. This can be problematic for some applications, because this will severely restrict the output peak voltage.

Our novel approach for addressing these problems is to construct a nano-structured MSM photodetector, consisting of a set of interdigitated fingers with rows of nanodots between the fingers to maintain a low capacitance without increasing the transit distance. For a given minimum feature size, this structure results in a larger operating bias voltage and also a larger peak output voltage.

2. Device Design and Fabrication

A conventional MSM photodetector is essentially composed of pairs of Schottky diodes connected back to back as shown in Fig. 1. The MSM photodetector with interdigitated electrodes is widely known to have a low capacitance per area, and typically its capacitance is approximately half of that of a p–i–n diode with similar quantum efficiency.[7]

We use semi-insulating GaAs for the MSM photodetectors in this work because of its optical absorption properties and high saturation velocity. As mentioned earlier, the RC constant of a device can still affect its speed, and this term should be included in the design. The MSM photodetector's overall 3 dB bandwidth is calculated with the following equation:

$$f_{3\mathrm{dB}} = \frac{1}{2\pi\tau}, \tag{1}$$

where

$$\tau = \tau_{\mathrm{transit}} + \tau_{\mathrm{RC}}, \tag{2}$$

and τ_{RC} and τ_{transit} are the RC time constant and the intrinsic transit time, respectively. For calculations of τ_{RC}, a load resistance of 50 Ω and a capacitance of the photodetector, C, are used. C is calculated with a metal-to-metal capacitance per unit length, C_0, of 0.03 fF/μm in the quation.[3]

$$C = C_0(N-1)L_{\mathrm{PD}}, \tag{3}$$

where N is a number of fingers, and L_{PD} is the length of one side of our square device. Also, it is assumed that electrons are traveling at their saturation velocity of GaAs, 2×10^7 cm/s.

We used the above analysis to generate Fig. 2, which provides the calculated bandwidth of the device in Fig. 1 as a function of device area. Figure 2 shows that bandwidths as high as 1 THz can be obtained by making detector area very small ($2 \times 2\,\mu\mathrm{m}^2$) with tight (80 nm) spacing between the interdigitated electrodes, as this reduces both the parasitic RC time and the transit time. The implication however, is that the operating bias voltage is quite low (1 V), thus restricting the peak output voltage to much lower levels. Having a much higher peak voltage is necessary for some applications, and is also an advantage for most applications.

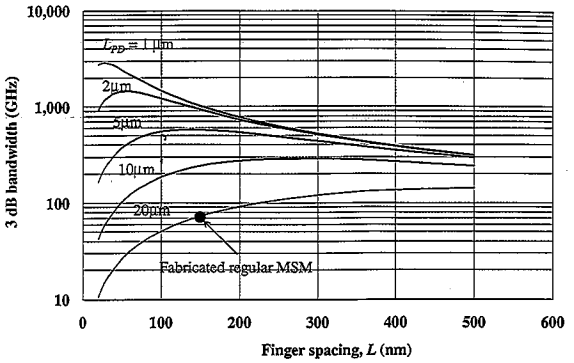

Fig. 2. (Color online) The calculated bandwidth of a GaAs MSM photodetector as a function of finger spacing, L, and detector size, L_{PD}.

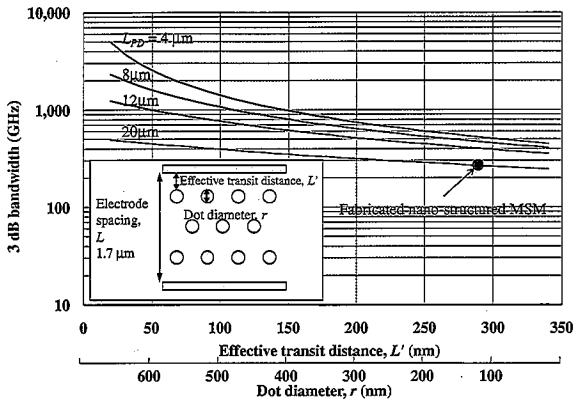

Fig. 3. (Color online) The calculated bandwidth of a nano-structured GaAs MSM photodetector as a function of dot diameter r, and detector size L_{PD}.

Our novel approach for addressing this problem is to construct a nano-structured MSM detector with rows of metal nanodots between the fingers. The nanodots act as artificial recombination centers at the surface, and are added to trade bandwidth, signal amplitude and efficiency. This structure can achieve an extremely short (<1 ps) transit time without increasing the RC time constant: The transit time is determined by the effective transit distance between the dots, L', while the capacitance depends on the total finger length, $(N-1)L_{\mathrm{PD}}$. Figure 3 shows the calculated bandwidth of an MSM photodetector as a function of the dot diameter, r, and the detector size, L_{PD}. As the metal dot diameter increases, the effective transit distance between an electrode and a dot, L', is reduced as shown in the inset of Fig. 3. Only photogenerated carriers that can reach the electrodes can contribute to the output signal. A bandwidth higher than 1 THz can be obtained with an $8 \times 8\,\mu\mathrm{m}^2$ detector and a 100 nm effective spacing or a $4 \times 4\,\mu\mathrm{m}^2$ detector and a 150 nm effective spacing because the MSM photodetector is no longer RC time limited, in contrast with conventional photodetectors shown in Fig. 2. In this model, an electrode spacing of 1.7 μm is used, and this should allow us to use a much higher bias voltage.

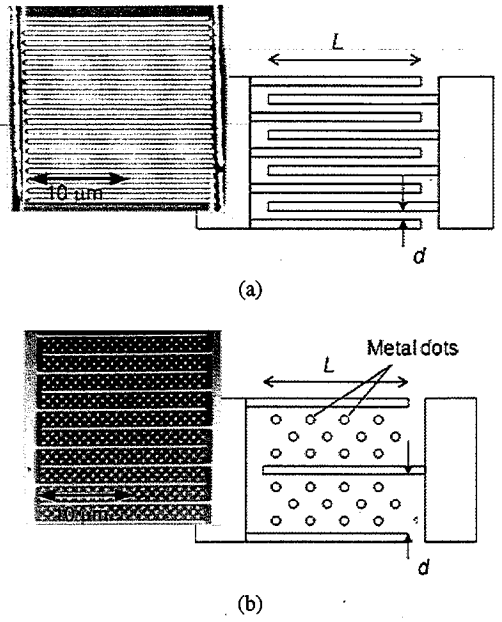

Fig. 4. (Color online) Layout and AFM image of (a) a regular MSM photodetector (width/spacing: 350 nm/150 nm) and (b) a nano-structured MSM photodetector (width/spacing: 300 nm/1800 nm; dot diameter: 300 nm).

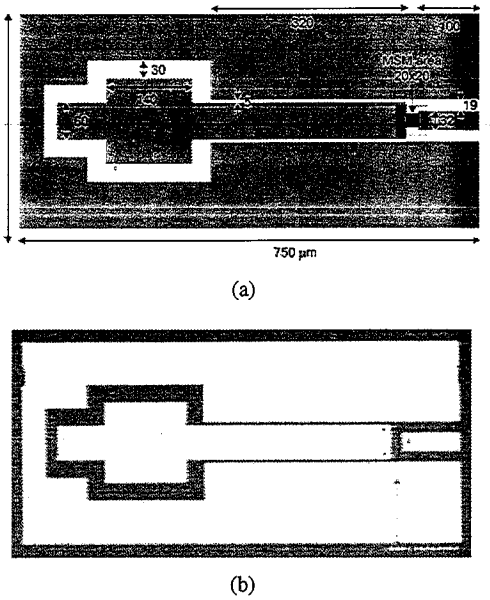

Fig. 5. (Color online) GSG transmission line and contact pad layout connecting the photodetector: (a) design and (b) optical micrograph. The device is biased on the left and the output is probed on the right.

Two distinctly different MSM photodetector structures have been designed, fabricated, and tested: A conventional MSM photodetector with interdigitated electrodes and a nano-structured MSM photodetector with three rows of metal dots. The layout and AFM image for a regular and a nano-structured MSM detector are presented in Fig. 4. The device area is $20 \times 20\,\mu m^2$ for both detectors.

The photodetectors were fabricated with 20 keV electron beam lithography on a semi-insulating GaAs substrate. The structure consists of a set of interdigitated 5 nm/30 nm Ti/Au thick fingers deposited by lift-off with a 100 nm/100 nm thick MMA–MAA copolymer [poly(methyl methacrylate/methacrylic acid)]/PMMA [poly(methyl methacrylate)] resist. The use of a double layer electron beam resist facilitates the metal lift-off process. Because MMA–MAA copolymer is more sensitive to electron beam exposure than PMMA, the double layer resist provides a better lift-off profile, while the PMMA top layer defines the resolution of the lithography.

The fabricated MSMs used for pulse response tests have the following dimensions: finger width/spacing of 350 nm/150 nm for the regular MSM photodetector, and 120 nm/1880 nm for the nano-structured MSM photodetector, which also includes three rows of 100 nm diameter dots. The area cover by metal is 30% for the regular MSM and 80% for the nano-structured MSM. The estimated internal bandwidth for the regular MSM is 70 GHz (indicated as a circle in Fig. 2), and above 200 GHz for the nano-structured MSM (in Fig. 3).

In order to enable pulse response measurements, the detectors were integrated with an on-chip ground–signal–ground (GSG) coplanar transmission line as illustrated in Fig. 5. The impedance of the transmission line on the left of the MSM detector is 30 Ω while that on the right is 50 Ω. This layer was placed by a separate lithography step followed by lift-off process of 5 nm/100 nm Ti/Au layer.

3. Experimental Results and Discussion

The DC measurements of a fabricated device show a typical photodetector behavior as shown in Fig. 6(a). As the amount of optical input power increases, the photocurrent becomes larger. In Fig. 6(b), the photocurrent density of the regular MSM and nano-structured MSM are measured under the same light input. The calculated responsivity is 0.12 for the regular MSM detector and 0.24 for the nano-structured MSM detector.

The DC measurement of the dark current (Fig. 7) reveals that the bias voltage (18 V) of the nano-structured MSM at which a dark current reaches 2 nA is three times larger than that of the regular MSM structure (6 V). As mentioned earlier, this result confirms that the nano-structured MSM photodetector can be operated at higher bias voltages than the regular MSM photodetector. The corresponding field strength for these devices is calculated to be 3.3×10^5 for the regular MSM and 1.0×10^5 V/cm for the nano-structured MSM. The values are lower than the published breakdown field strength of GaAs,[8] and this indicates that the breakdown of the device is caused by the surface leakage current.[9]

The pulse response of the devices is obtained by applying 100 fs optical pulses with 775 nm wavelength and up to 100 W peak power. The resulting electrical signal is measured using a GSG probe and an oscilloscope with 70 GHz bandwidth. The pulse response shown in Fig. 8 illustrates that the nano-structured MSM photodetector biased at 5.0 V has a 3.6 times larger peak amplitude than the regular MSM biased at 1.5 V and that with a slightly smaller pulse width. The full width half maximum (FWHM) values are approximately 10 ps. The nano-structured MSM detector should have a much shorter internal pulse response, but the output signal is significantly broadened by the limited oscilloscope bandwidth.

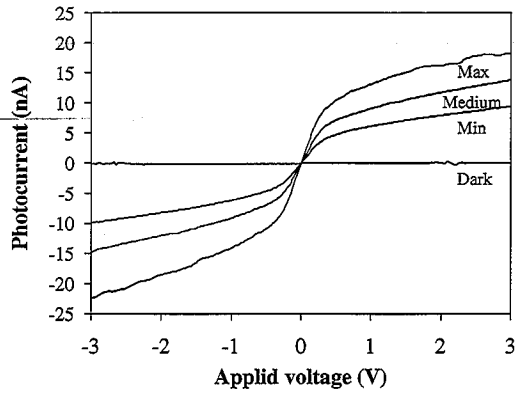

(a)

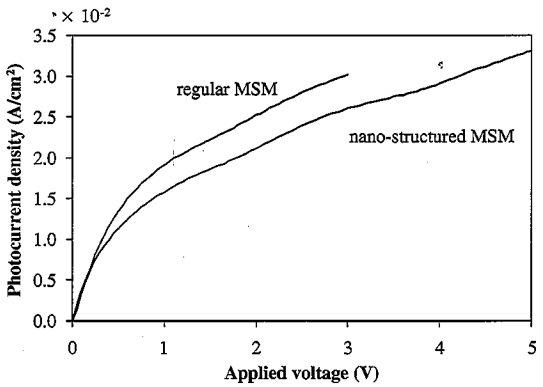

(b)

Fig. 6. Photocurrent measurements: (a) the regular MSM without transmission line at different levels of optical input and (b) photocurrent density comparison between the regular MSM and nano-structured MSM under the same optical input.

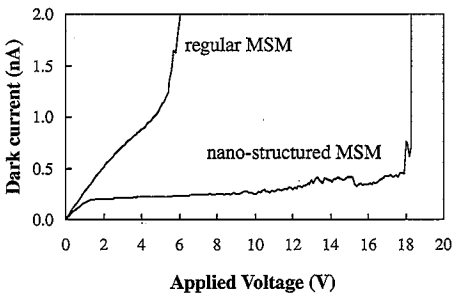

Fig. 7. Comparison of the dark current of the MSM and nano-structured MSM photodetector.

The measurement of the peak voltage as function of the bias voltage for the nano-structured MSM reveals that the peak amplitude scales with the operating voltage, while the optical input power is not changed. In order to analyze this behavior, a simple model of a MSM photodetector is constructed based on standard rate equations for the electron density within the MSM detector:

$$\frac{dN_{\mathrm{ph}}}{dt} = -\frac{N_{\mathrm{ph}}}{\tau} - BN_{\mathrm{ph}}{}^2 - \frac{I_{\mathrm{MSM}}}{q} + \frac{P_{\mathrm{opt}}}{E_{\mathrm{ph}}}, \tag{4}$$

where N_{ph} is the photogenerated carrier concentration, B is

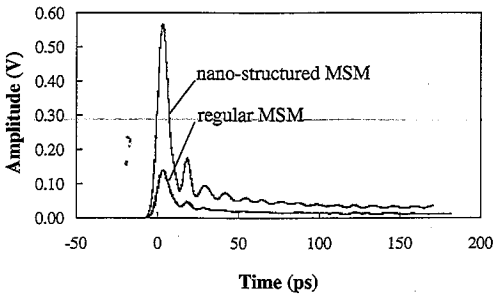

Fig. 8. Pulse response of the regular MSM photodetector biased at 1.5 V compared to that of the nano-structured MSM photodetector biased at 5 V.

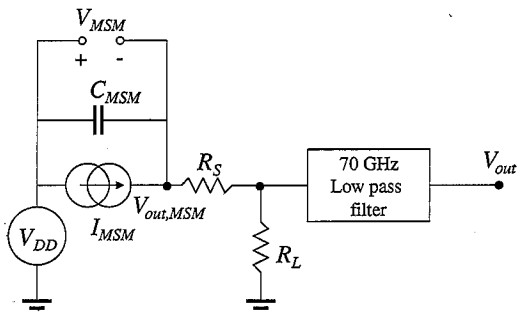

Fig. 9. Equivalent circuit model of measurement system simulation.

the bimolecular recombination constant, τ is the effective recombination time, P_{opt} is the optical input power, and E_{ph} is the photon energy. The total MSM current that depends on this electron density is expressed as

$$I_{\mathrm{MSM}} = \frac{q\mu N_{\mathrm{ph}} V_{\mathrm{MSM}}}{L'L}, \tag{5}$$

where μ is the electron mobility, L is the distance between electrodes, and L' is the effective transit distance as shown in Fig. 3. Velocity saturation is not included in this model. The MSM voltage V_{MSM} is then obtained from the equivalent circuit model shown in Fig. 9, and the equation:

$$I_{\mathrm{MSM}} + C_{\mathrm{MSM}}\frac{dV_{\mathrm{MSM}}}{dt} = \frac{V_{\mathrm{DD}} - V_{\mathrm{MSM}}}{R_{\mathrm{S}} + R_{\mathrm{L}}}. \tag{6}$$

V_{out} is the output voltage measured with an oscilloscope, as shown in Fig. 9. The oscilloscope is treated as a 70 GHz low pass filter in this model, combined with a load resistance, R_{L}, of 50 Ω. A series resistance, R_{S}, of 175 Ω is also included to model the resistance of the thin (30 nm) MSM fingers.[10]

The simulated pulse response of the nano-structured MSM photodetector model as a function of bias voltage is shown in Fig. 10. As can be seen in the figure, the peak output voltage is limited by the power supply voltage, V_{DD}. This is because a decrease in the voltage across the MSM photodetector, V_{MSM}, is closely related to $V_{\mathrm{out,MSM}}$, which cannot exceed V_{DD}. The low pass filter changes the shape of the pulse, but does not affect the V_{DD} dependence of the peak output voltage. As the optical power is increased, the photocurrent increases until the voltage across the total resistance, $R_{\mathrm{L}} + R_{\mathrm{S}}$, reaches V_{DD}. The photocurrent remains until all carriers disappear through recombination and/or diffusion. Because the power supply

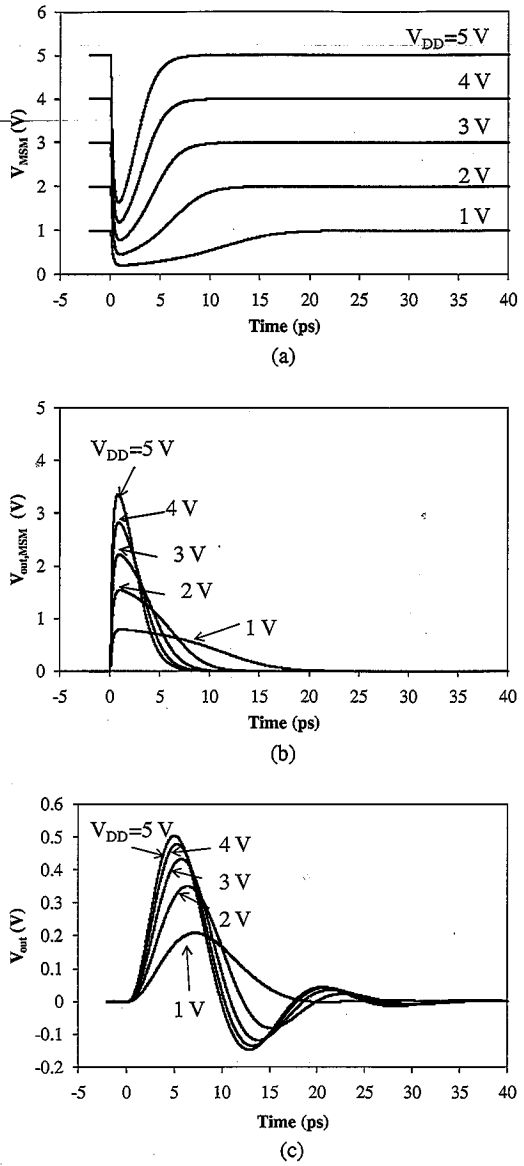

Fig. 10. The simulation results of (a) V_{MSM}, (b) $V_{out,MSM}$, and (c) V_{out} as a function of time with V_{DD} as a parameter. Peak input optical power is 100 W and the optical pulse is assumed to be triangular with a full width half max of 0.1 ps.

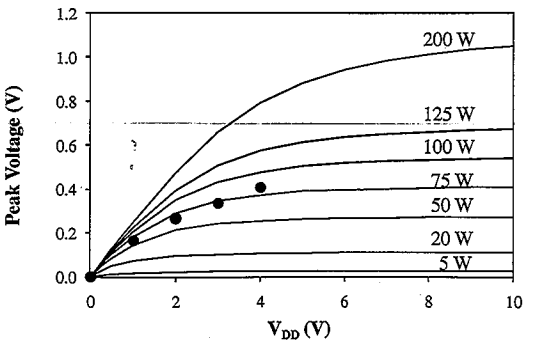

Fig. 11. The simulated peak voltage as a function of bias voltage and input peak optical power.

voltage is divided between the resistors and the detector, at high photocurrents the resistive voltage drop dominates and the voltage across the detector drops to near zero, an effect called "voltage collapse".

The simulated peak voltage of a nano-structured MSM photodetector at different optical power levels is shown in Fig. 11. According to the simulation, the nano-structured MSM model demonstrates a saturation of the photocurrent with increasing supply voltage at low optical input level. As the optical power is increased, the saturation occurs at higher power supply voltage and no saturation is observed in the entire operating range when the input power is above 1 kW. The measured output peak voltages do not saturate between 0 and 5 V, as the observed signal amplitude increases with bias voltage. As shown in Fig. 11, the data follow the calculated voltage at an optical peak power of 75 W reasonably well.

We conclude that the transit model explains the main features of the measured pulse response of nano-structured MSM photodetectors. The output peak voltage is limited by V_{DD} at high optical power level, as the response is strongly influenced by the voltage collapse effect.

4. Conclusions

A novel nano-structured MSM photodetector has been fabricated and tested.

The nano-structured MSM photodetector has been operated at a bias voltage of 5 V, more than three times higher than that of a regular MSM photodetector. Its dark current is much lower until the bias voltage approaches to the breakdown field. More importantly, it demonstrates a more than three times higher peak voltage output while maintaining approximately a 10 ps pulse width, which is limited by the bandwidth of the measurement setup, not that of nano-structured MSM photodetector. This study provides a basis for future development of high speed, high voltage MSM photodetectors. The simulations also indicate that the pulse response at high optical power levels is strongly influenced by the voltage collapse across the photodetector.

Acknowledgements

We thank Jan Van Zeghbroeck for his support. This project is supported in part by CU-NIST Seed Grand 2007.

1) L. Xu, G. Tempea, Ch. Spielmann, F. Krausz, A. Stingl, K. Ferencz, and S. Takano: Opt. Lett. **23** (1998) 789.
2) E. R. Brown, K. A. McIntosh, K. B. Nichols, and C. L. Dennis: Appl. Phys. Lett. **66** (1995) 285.
3) S. Y. Chou and M. I. Liu: IEEE J. Quantum Electron. **28** (1992) 2358.
4) R. A. Lawton and A. Scavannec: Electron. Lett. **11** (1975) 74.
5) L. Y. Lin, M. C. Wu, T. Itoh, T. A. Vang, R. E. Muller, D. L. Sivco, and A. Y. Cho: IEEE Trans. Microwave Theory Tech. **45** (1997) 1320.
6) B. J. Van Zeghbroeck, W. Patrick, J. Halbout, and P. Vettiger: IEEE Electron Device Lett. **9** (1988) 527.
7) S. M. Sze: *Physics of Semiconductor Devices* (Wiley, New York, 2007) 3rd ed., p. 712.
8) J. Singh: *Semiconductor Devices: Basic Principles* (Wiley, New York, 2001) p. 102.
9) A. Gin, Y. Wei, J. Bae, A. Hood, J. Nah, and M. Razeghi: Thin Solid Films **447–448** (2004) 489.
10) P. Švorčík, J. Zehebtber, V. Rybka, P. Slepička, and V. Hnatowcz: Appl. Phys. A **75** (2002) 541.